Journal of Inorganic Biochemistry 105 (2011) 927–936

Contents lists available at ScienceDirect

Journal of Inorganic Biochemistry

journal homepage: www.elsevier.com/locate/jinorgbio

# Tungsten-dependent formaldehyde ferredoxin oxidoreductase: Reaction mechanism from quantum chemical calculations

Rong-Zhen Liao [a,b], Jian-Guo Yu [b], Fahmi Himo [a,*]

[a] Department of Organic Chemistry, Arrhenius Laboratory, Stockholm University, SE-10691 Stockholm, Sweden
[b] College of Chemistry, Beijing Normal University, Beijing, 100875, People's Republic of China

ARTICLE INFO

*Article history:*
Received 17 January 2011
Received in revised form 25 March 2011
Accepted 28 March 2011
Available online 5 April 2011

*Keywords:*
Tungstoenzyme
Formaldehyde oxidoreductase
Reaction mechanism
Density functional theory
Enzyme catalysis

ABSTRACT

Formaldehyde ferredoxin oxidoreductase from *Pyrococcus furiosus* is a tungsten-dependent enzyme that catalyzes the oxidation of formaldehyde to formic acid. In the present study, quantum chemical calculations are used to elucidate the reaction mechanism of this enzyme. Several possible mechanistic scenarios are investigated with a large model of the active site designed on the basis of the X-ray crystal structure of the native enzyme. Based on the calculations, we propose a new mechanism in which the formaldehyde substrate binds directly to the tungsten ion. $W^{VI}$=O then performs a nucleophilic attack on the formaldehyde carbon to form a tetrahedral intermediate. In the second step, which is calculated to be rate limiting, a proton is transferred to the second-shell Glu308 residue, coupled with a two-electron reduction of the tungsten ion. The calculated barriers for the mechanism are energetically very feasible and in relatively good agreement with experimental rate constants. Three other second-shell mechanisms, including one previously proposed based on experimental findings, are considered but ruled out because of their high barriers.



## 1. Introduction

Tungsten is the heaviest chemical element in biology, and plays essential roles in biological carbon, nitrogen, and sulfur metabolisms [1–8]. In tungsten-dependent enzymes, the tungsten ion has an oxidation number varying from +4 to +6 and is seen to be bound to pterin cofactors. On the basis of sequence homology, cofactor composition, metal coordination, and the nature of the axial ligands, tungsten enzymes have been divided into three different families: aldehyde oxidoreductases (AORs), formate dehydrogenases (FDHs), and acetylene hydratases (AHs) [1]. The former two catalyze redox reactions, while the latter catalyzes a non-redox hydration of acetylene. In *Pyrococcus furiosus*, five members of the AOR family have been purified and characterized: aldehyde ferredoxin oxidoreductase (also abbreviated AOR) [9,10], formaldehyde ferredoxin oxidoreductase (FOR) [11], glyceraldehyde-3-phosphate ferredoxin oxidoreductase (GAPOR) [12,13], tungsten-containing oxidoreductase number four (WOR4) [14], and tungsten-containing oxidoreductase number five (WOR5) [15]. All these enzymes are oxygen-sensitive and have optimal activities at about 80 °C [16].

The crystal structures of both AOR and FOR have been solved and they revealed that the tungsten ion is bound to two pterins in the active site [17,18]. They share about 40% amino acid sequence identity and have quite similar active site structures. FOR is a homotetramer and the tungsten ion is ligated by the four sulfur atoms of the two pterin dithiolene moieties and an oxygen species, presumably an oxo group (Fig. 1) [18]. It has been suggested that an additional water molecule occupies the empty coordination site [18]. A mechanistically important second-shell residue, Glu308, is found to form two hydrogen bonds to Tyr416 and the Ser414–Gly415 peptide backbone. Another second-shell residue, His437, donates hydrogen bond to the dithiolene sulfur and forms an additional hydrogen bond to Ser414.

The redox properties of the tungsten center in AORs from *P. furiosus* and *Pyrococcus* strain ES-4, and FORs from *Thermococcus litoralis* and *P. furiosus* have been investigated by EPR redox titrations [19–24]. A redox cycle between $W^{IV}/W^{V}$ and $W^{V}/W^{VI}$ has been characterized through EPR spectrum of $W^{V}$, which has a doublet electronic configuration. The redox potential of *P. furiosus* FOR was suggested to be significantly lower than −400 mV [23]. Furthermore, the formaldehyde substrate was proposed to be oxidized by $W^{VI}$ with a two-electron transfer to the metal center affording $W^{IV}$. The two electrons are then transferred to the ferredoxin cofactors, regenerating the $W^{VI}$ species [24].

Since tungsten and its lighter congener molybdenum in the periodic table group 6 have quite similar chemical properties, it is not surprising that some enzymes can adopt both elements for their activities, like, for example, dimethyl sulfoxide reductase [25], trimethylamine N-oxide reductase [26], formylmethanofurane dehydrogenase [27,28], and acetylene hydratase [29]. However, some other enzymes are strictly dependent on either tungsten or molybdenum. For example, metal exchange experiment for tungsten-dependent

* Corresponding author.
*E-mail address:* himo@organ.su.se (F. Himo).

0162-0134/$ – see front matter © 2011 Elsevier Inc. All rights reserved.
doi:10.1016/j.jinorgbio.2011.03.020

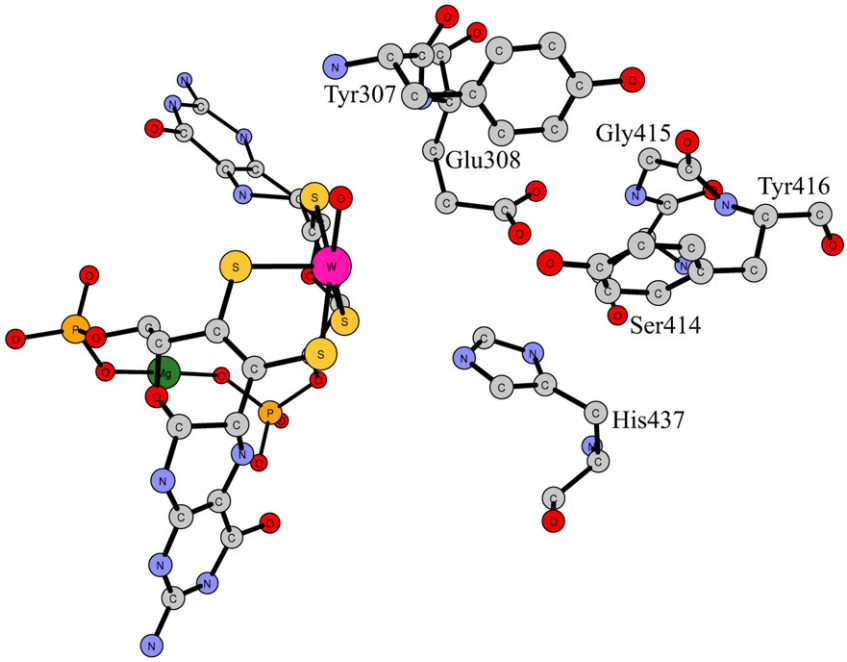


**Fig. 1.** X-ray crystal structure of FOR active site. (Coordinates taken from PDB entry 1B25) [18].

AOR (W-AOR) from *P. furiosus* showed that molybdenum can be incorporated into the active site but without any catalytic activity [7].

A molybdenum-dependent AOR (Mo-AOR) from *Desulfovibrio gigas* has also been purified and it was suggested to belong to the xanthine oxidase family [30–33]. Amino acid sequence comparison and crystal structural analysis show that this enzyme is not related to the tungsten-dependent FOR or AOR, even though they catalyze the same kind of reactions [18]. In the active site, the Mo ion is bound to one pterin cytosine dinucleotide, two oxygen species and a sulfur species [33]. A second-shell residue, Glu869, forms one hydrogen bond to the oxygen species bound to Mo. The reaction mechanisms of Mo-AOR [34], xanthine oxidase [35–44], and other related Mo-dependent enzymes [45–53] have been studied using quantum chemical methods. Recent QM/MM calculations of Mo-AOR suggested that the Glu869 residue functions as a general base to take a proton from the Mo-OH and to facilitate nucleophilic attack on the substrate aldehyde carbonyl carbon to form a tetrahedral intermediate [34]. In the following step, an intramolecular hydride transfer from the intermediate diol carbon to the sulfido occurs through a five-membered transition state.

A mechanistic proposal for the formaldehyde oxidation in W-FOR has emerged on the basis of crystal structure and by analogy to the mechanisms of Mo-AOR and xanthine oxidase [18]. Glu308 is proposed to activate a water molecule to attack the substrate carbonyl group to form a tetrahedral intermediate. In the second step, a hydride transfer to $W^{VI}$=O occurs, coupled with two-electron transfer to W center to generate $W^{IV}$ [18].

In the present study, density functional calculations are employed to elucidate the reaction mechanism of W-FOR. A Cluster model of the active site is designed on the basis of the crystal structure, and the hybrid density functional B3LYP [54,55] is used to calculate the potential energy profiles for several different mechanistic scenarios. The quantum chemical cluster approach for studying enzymatic reactions has previously been applied to a wide spectrum of enzymes [56–63]. Indeed, many mechanistic problems have been solved using this approach, and a wealth of new insight has been gained. In particular, similar quantum chemical calculations were very recently employed to elucidate the reaction mechanism of the aforementioned tungsten-dependent enzyme acetylene hydratase [64].

## 2. Computational details

All calculations were performed using the Gaussian03 program [65] with the B3LYP [54,55] functional. For geometry optimizations, the 6–31 G(*d,p*) basis set was used for the C, N, O, and H elements, the 6–311 + G(*d*) for S, and the LANL2TZ(*f*) pseudopotential [66] for W. For W, scalar relativistic effects are included through the use of relativistic pseudopotential. Spin-orbit coupling effects were not explicitly considered. We have calculated both the singlet and triplet states for all stationary points. Although spin-orbit effects could lower the energy of the triplet state somewhat [67,68], it will not alter any mechanistic conclusions. Based on the optimized geometries, final energies were evaluated with the larger basis set 6–311 + G(*2 d,2p*) for C, N, O, S, H atoms and the LANL2TZ(*f*) basis set for metal. Zero-point energy (ZPE) effects were computed by performing analytical frequency calculations at the same level of theory as the geometry optimizations. As will be discussed below, certain atoms were kept fixed to their X-ray crystal positions during geometry optimizations. This leads to several small imaginary frequencies, in this case on the order of 10*i*–40*i* $cm^{-1}$. As they do not contribute significantly to the ZPE, they can be ignored. Large active site models, like the one used in the present study, can suffer from multiple minima problems, which can lead to unreliable relative energies. By careful visual inspection we have done our best to confirm that the parts that do not directly participate in the reaction are in the same local minima throughout the reaction. To some extent, the coordinate locking procedure adopted here facilitates this task. We have also made sure that the obtained transition states indeed connect the correct reactants and products.

To account for the polarization effects of the protein environment that is not explicitly included in the quantum chemical model, single-point calculations on the optimized structures were carried out with the conductor-like polarizable continuum model (CPCM) [69–72] at the same level of theory as geometry optimizations. The dielectric constant was chosen to be 4, which is a standard value used in modeling protein surroundings. Recent studies from our laboratory on several different classes of enzymes have shown that the dielectric effects of the surrounding diminish with increasing model size [73–75]. At a model size of ca 150–200 atoms, the solvation effects almost

vanish and the choice of the dielectric constant thus becomes rather insignificant. The energies below are reported with and without solvation effects.

## 3. Active site model

To investigate the various reaction pathways, a quantum chemical model of the FOR active site was devised on the basis of the crystal structure of the native enzyme (PDB entry 1B25) [18]. The first coordination shell of the tungsten was represented by two 2-methylpyranedithiolenes that mimic the pterin cofactors, an oxo and a water molecule (Fig. 2). Truncated models of the second-shell residues Tyr307–Glu308, Ser414–Gly415, Tyr416 and His437 were also included, as shown in Fig. 2. Hydrogen atoms were added manually. To keep the optimized structures close to the experimental one, some truncated atoms were kept fixed at their corresponding X-ray positions during the geometry optimizations. These atoms are labeled with asterisks in the figures below. The natural formaldehyde substrate was used to study the mechanism. The resulting model consists of 104 atoms. The oxidation state of W is +6, which is believed to be the reactive state [24], and thus the total charge of this model is −1.

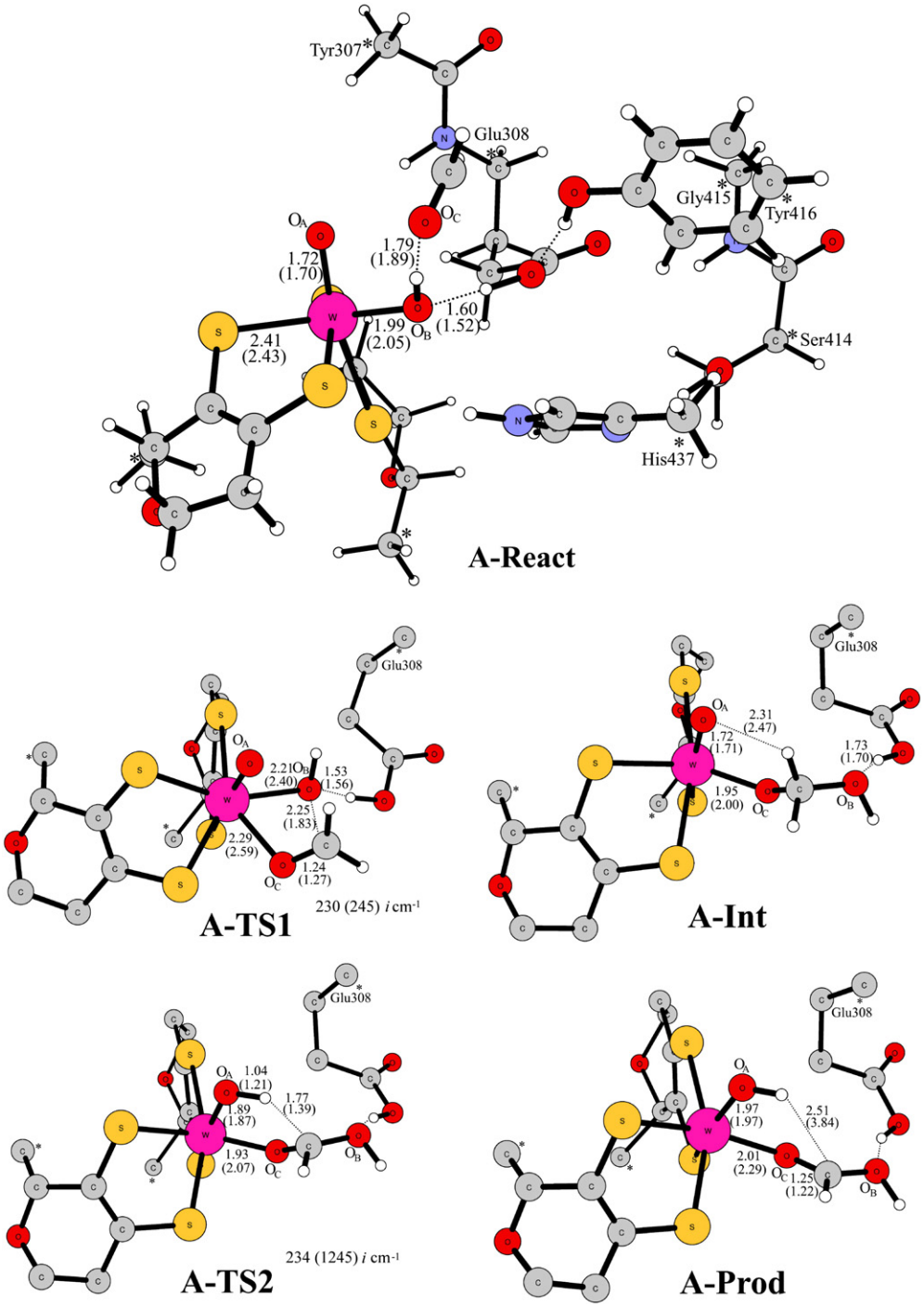


**Fig. 2.** Optimized structures of stationary points along pathway A for the active site model of FOR. Atoms with asterisks were fixed at their X-ray structure positions during the geometry optimizations. Distances are given in angstrom (Å) for the singlet state (triplet in parentheses). For clarity, the full model is shown only for *A-React*. For the other stationary points, some residues and hydrogen atoms are omitted. For transition states the imaginary frequency is indicated (triplet in parentheses).

## 4. Results and discussion

In the search of an energetically plausible reaction mechanism, several mechanistic scenarios were considered in this study. They are labeled as pathways *A*, *B*, *C*, and *D* as shown in Scheme 1. Pathway *A* is the previously suggested one based on experimental studies, while pathways *B*, *C*, and *D* are new proposals made in the present study.

### 4.1. Pathway A

First, we investigate the previously proposed mechanism (pathway *A* in Scheme 1), in which the Glu308 residue activates the W-bound water molecule to make a nucleophilic attack on the substrate carbonyl carbon. This is then followed by a hydride transfer to $W^{VI}=O$ [18]. In the reaction, the tungsten changes its oxidation state from +6 to +4 and electronic configuration from $d^0$ to $d^2$. As the multiplicity of the tungsten species could change during the reaction, we explored the mechanism for both the singlet and triplet states. The optimized structure of the active site model in complex with formaldehyde in pathway *A* (*A-React*) is displayed in Fig. 2. The geometry optimization was initially started with a neutral water molecule bound to W and a negatively-charged Glu308. However, during the optimization, a proton was transferred automatically from the water to Glu308 to form a neutral Glu308 residue. The tungsten ion is hexa-coordinated and the $W=O_A$ and $W-O_BH$ distances are 1.72 and 1.99 Å, respectively. A hydrogen bond can be observed between Glu308 and tungsten-bound hydroxide, with an O···H distance of 1.60 Å. The formaldehyde substrate in the second shell is hydrogen-bonded to the hydroxide with a hydrogen bond distance of 1.79 Å. At *A-React*, the triplet state is calculated to be 18.8 kcal/mol higher than the singlet state (18.6 kcal/mol without the solvation correction).

Starting from *A-React*, we have optimized the transition state for the nucleophilic attack (*A-TS1*) and the resulting intermediate (*A-Int*) (see Fig. 2). The barrier is calculated to be 34.2 kcal/mol in the singlet

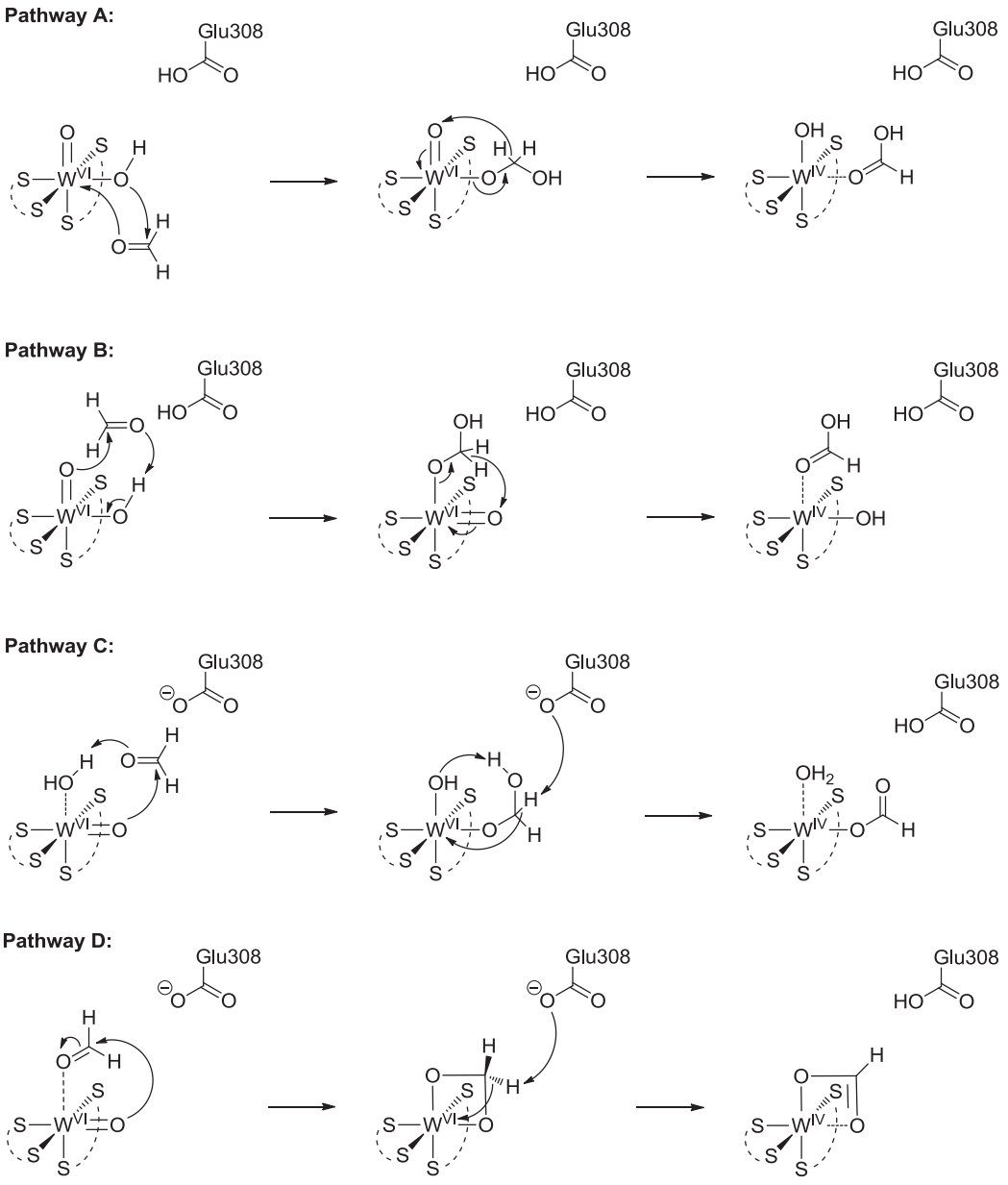


**Scheme 1.** Four possible mechanisms for W-FOR investigated in the present study.

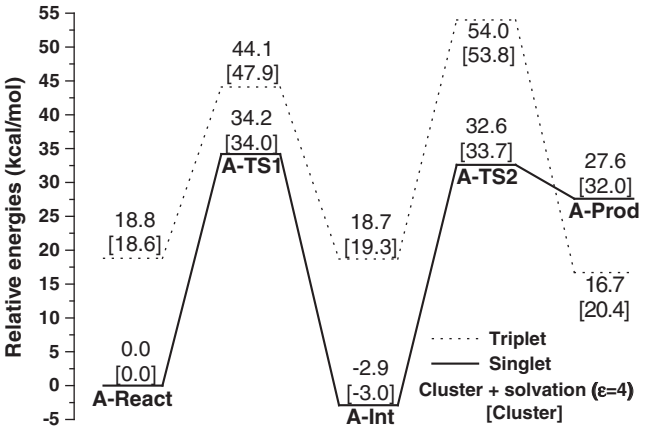


**Fig. 3.** Calculated potential energy profile for pathway *A*. Values in the square brackets are without solvation correction.

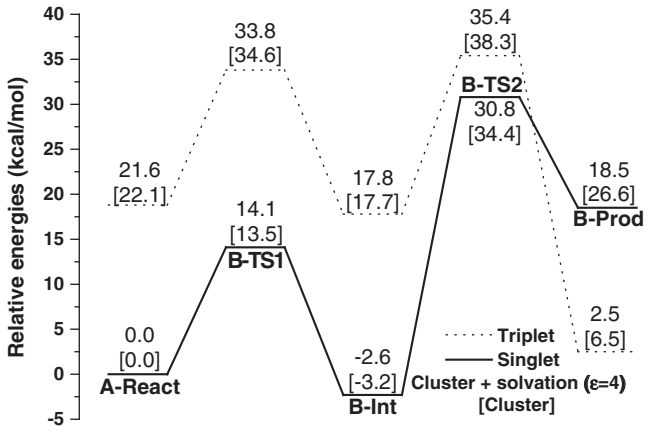


**Fig. 5.** Calculated potential energy profile for pathway *B*.

state and 44.1 kcal/mol in the triplet state relative to singlet *A-React*. *A-Int* lies at −2.9 kcal/mol in singlet state and +18.7 kcal/mol in triplet state. The reason for the high barrier is that at *A-TS1*, the tungsten becomes hepta-coordinated in order to switch the ligands (Fig. 2). The distance of the forming C–$O_B$ is 2.25 Å, while the W–$O_B$ and W–$O_C$ distances are 2.21 and 2.29 Å, respectively.

The following step, involving a hydride transfer to the W-oxo group, coupled with the two-electron reduction of the tungsten, turns out to also have a very high barrier. The transition state for this step was located (called *A-TS2*) and is shown in Fig. 2. The calculated energies of *A-TS2* are 32.6 kcal/mol in the singlet state and 54.0 kcal/mol in the triplet state compared to singlet *A-React*. The resulting structure corresponds to the tungsten cluster in complex with the formic acid product (*A-Prod*, Fig. 2). The energies of this complex are calculated to be 27.6 kcal/mol in the singlet state and 16.7 kcal/mol in the triplet state higher than that of singlet *A-React*.

The reason for the high barrier may be that the W-oxo here is a poor hydride acceptor. In Mo-AOR, an Mo-sulfido is used to accept the hydride. QM/MM calculations show that the barrier for hydride transfer to sulfido is about 15 kcal/mol lower than that to Mo-oxo [43].

Our calculations show thus that the energies of pathway *A* (summarized in Fig. 3) are prohibitively high for this mechanism to be a viable option. As seen from Fig. 3, a spin crossing can take place during the product formation step. However, since the barriers for the mechanism are very high, this issue becomes irrelevant.

An alternative concerted pathway can also be envisioned, in which the nucleophilic attack and the hydride transfer occur simultaneously. QM/MM calculations of Mo-AOR show that this mechanism has a barrier of 20.2 kcal/mol, which is higher than the stepwise pathway for that enzyme [34]. In the present study, we have also considered this possibility. The barrier is calculated to

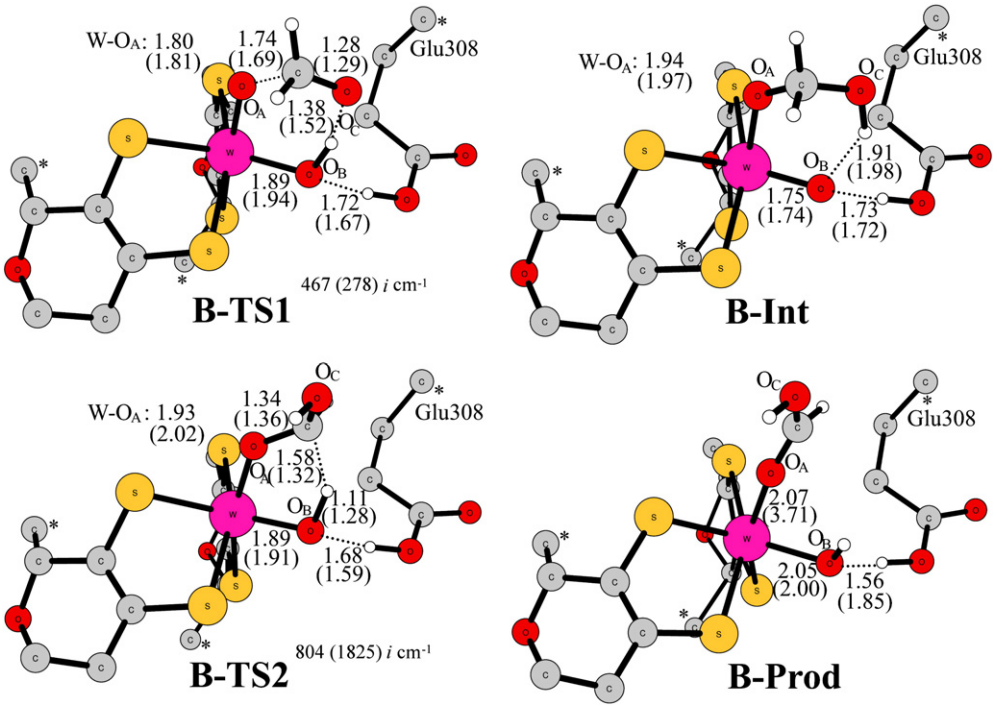


**Fig. 4.** Optimized geometries of stationary points along reaction pathway *B*. For clarity, some residues and hydrogen atoms are omitted.

be extremely high, 53.8 kcal/mol for the singlet state and 58.4 kcal/mol for the triplet state, ruling out this possibility as well. The optimized transition state is shown in the Supporting Information (Fig. SI1).

### 4.2. Pathway B

We now consider another mechanistic possibility, in which the $W^{VI}$=O acts as the nucleophile and the tungsten-bound hydroxide ($O_BH$ ) protonates the formaldehyde oxygen. This is then followed by a hydride transfer to $O_B$ (see Scheme 1). All stationary points along the reaction pathway for both singlet and triplet states were optimized and are displayed in Fig. 4. The calculated potential energy profile is shown in Fig. 5.

Starting from the same reactant structure as for pathway *A* (*A-React*), the geminal diol intermediate (*B-Int*) formation proceeds through a six-membered transition state (*B-TS1*). The barrier now is calculated to be 14.1 kcal/mol for singlet state, which is about 20 kcal/mol lower than that of *A-TS1*. Our calculations show thus that $W^{VI}$=O is a much better nucleophile than W–OH. Another important feature is that in this mechanism the tungsten avoids becoming hepta-coordinated as in *A-TS1*. The resulting *B-Int* lies at −2.6 kcal/mol relative to *A-React*. In *B-Int*, $O_B$ becomes the oxo group that in the next step accepts a hydride.

Similarly to *A-TS2*, the hydride transfer proceeds through a five-membered transition state (*B-TS2*). The barrier for this step is calculated to be 30.8 kcal/mol, which is also very similar to the barrier of the second step of pathway *A*.

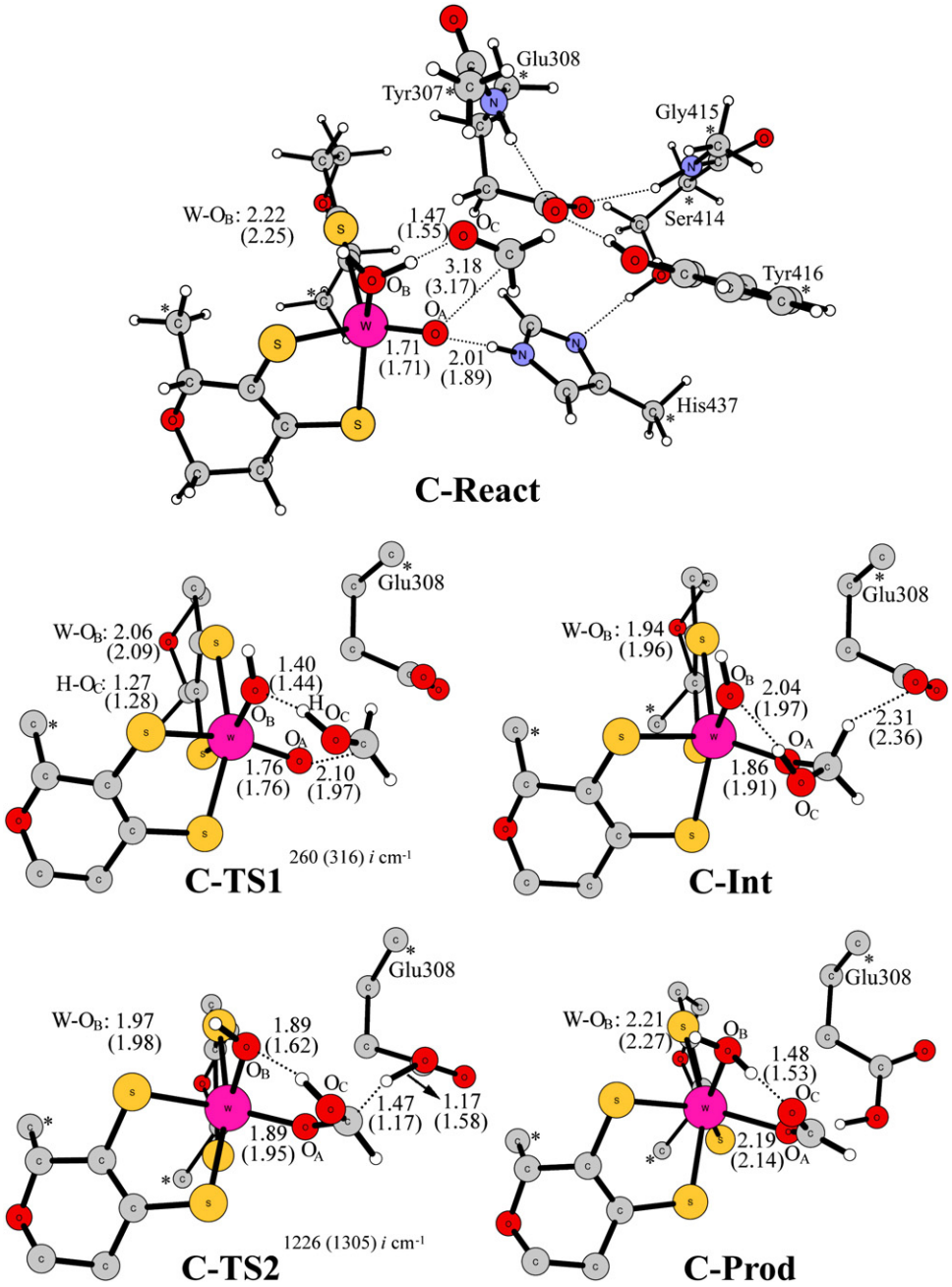


**Fig. 6.** Optimized geometries of stationary points along reaction pathway *C*. For clarity, the full model is shown only for *C-React*. For the other stationary points, some residues and hydrogen atoms are omitted.

These results show that the $W^{VI}$=O species is a good nucleophile capable of attacking the aldehyde. However, the following hydride transfer step is associated with a high barrier, which rules out this mechanistic possibility too.

### 4.3. Pathway C

In pathway B, a reasonable barrier was obtained for the first step, when the oxo performs the nucleophilic attack, but not for the hydride transfer step. Some other pathway thus has to be in action for the intermediate oxidation, and an alternative mechanistic scenario is that a base takes a proton and two electrons transfer to the metal center. This mechanism has been suggested for Mo-dependent formate dehydrogenase, for which DFT calculations show that a SeCys residue takes a proton from the substrate formate, simultaneously with a two-electron reduction of $Mo^{VI}$ [48]. The most likely candidate for the base in the case of W-FOR is Glu308. Here we consider this possibility (pathway *C*, Scheme 1).

In order for Glu308 to function as a base it has to be in the ionized form, i.e. the proton has to remain at the tungsten-bound water molecule in *A-React*. However, it is energetically favorable for the proton to be at the Glu308 residue, and the only way to avoid this was to switch places between the oxo and the hydroxide group in *A-React*. This results in the structure labeled as *C-React* in Fig. 6. The energy of *C-React* is calculated to be +10.9 kcal/mol for the singlet and +25.2 kcal/mol for the triplet compared to *A-React*. From *C-React*, we have optimized the transition state (*C-TS1*, Fig. 6) for the nucleophilic attack and the resulting tetrahedral intermediate (*C-Int*). Similarly to *B-TS1*, $W^{VI}$=O performs the nucleophilic attack and the tungsten-bound water molecule protonates the formaldehyde substrate in *C-TS1*. The barrier for this step is calculated to be 26.1 kcal/mol for the singlet and 42.3 kcal/mol for the triplet (Fig. 7) relative to *A-React*. *C-Int* lies at +13.9 kcal/mol (+26.7 kcal/mol for the triplet).

The following step is a proton transfer from the diol carbon to Glu308, coupled with a two-electron reduction of $W^{VI}$. The transition state (*C-TS2*) was optimized and is shown in Fig. 6. It was found that, simultaneously with the proton transfer to Glu308, the other proton is transferred back from $O_C$ to $O_B$. The calculated energy of *C-TS2* is 27.8 kcal/mol (singlet, Fig. 7) higher than that of *C-React*. This shows that even if *C-React* is not high in energy compared to *A-React*, the barrier for the second step makes pathway C an unlikely mechanistic option.

### 4.4. Pathway D

In all three mechanisms discussed so far the substrate binds in the second coordination shell of the tungsten ion. In pathway *D* we consider the situation when the substrate binds directly to the tungsten. A similar binding mode was recently suggested for acetylene hydratase, in which the acetylene substrate was calculated to bind directly to $W^{IV}$ in an $\eta^2$ fashion [64]. In the reactant complex *D-React* (Fig. 8), the formaldehyde carbonyl oxygen is coordinated to W with a distance of 2.40 Å. In the triplet state it is unbound, and the singlet-triplet gap is 9.9 kcal/mol.

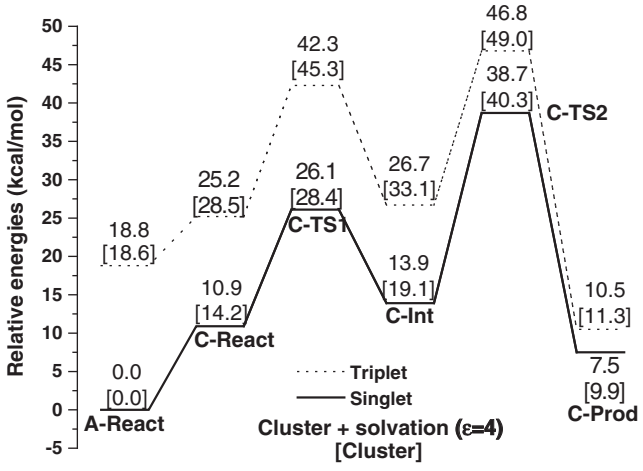


**Fig. 7.** Calculated potential energy profile for pathway *C*.

From *D-React*, the formaldehyde can easily undergo a nucleophilic attack by the W=O group with a barrier of 14.3 kcal/mol, which is very similar to the barrier found for the first step of pathway *B*. The optimized transition state (*D-TS1*) and the resulting intermediate (*D-Int*) are displayed in Fig. 8. At *D-TS1*, the nascent C-$O_A$ distance is 2.02 Å and the W=O bond is elongated to 1.77 Å. During the nucleophilic attack, the tungsten ion stabilizes the negative charge developed on the formaldehyde $O_C$, thereby lowering the barrier and the energy of the intermediate, which is calculated to be -2.1 kcal/mol relative to *D-React*. A similar charge-stabilizing role was also ascribed to the tungsten ion in the first-shell mechanism calculated for acetylene hydratase [64]. At *D-Int*, the two negatively charged oxygens ($O_A$ and $O_C$) are coordinated to W with similar bond distances, and one of the two protons attached to the diol carbon is pointing toward Glu308, with a distance of 2.12 Å. We then optimized the transition state for the proton transfer from the intermediate to Glu308 (*D-TS2*, Fig. 8). The barrier now is the very feasible 16.6 kcal/mol relative to *D-Int*. At *D-TS2*, the critical C–H and $O_{Glu308}$–H distances are 1.44 and 1.18 Å, respectively. This step is not a simple proton transfer between a C–H bond and a carboxylate, because concomitantly with the proton transfer, two electrons are transferred from the substrate to $W^{VI}$ to afford $W^{IV}$. At *D-Prod*, the formate product is coordinated to the metal center in a bidentate fashion, and the energy is −9.9 kcal/mol compared to *D-React*.

The potential energy profile for pathway *D* is summarized in Fig. 9. It can be seen that the singlet state is lower than the triplet throughout the whole reaction. The barrier for the second step is 16.6 kcal/mol relative to *D-Int*, which is 2.3 kcal/mol higher than the barrier of the first step, indicating that the second step is rate-limiting. The rate constant for formaldehyde oxidation has been experimentally measured to be in the range of 4–60 $s^{-1}$ at 80 °C [22,23]. This can be converted to barriers in the range of 18–20 kcal/mol using classical transition state theory. The calculated barrier for pathway *D* is thus in quite good agreement with the experimental rate constant, but somewhat underestimated. We have tested how sensitive the results are to the choice of functional. Single-point calculations using the BB1K functional [76] gave very similar barriers, with deviations of less than 2 kcal/mol.

Since pathway *D* is a first-shell mechanism, it is possible that the substrate has to displace one of the metal ligands (in this case a water molecule) to reach the active species *D-React*. In general, ligand exchange energies at enzyme active sites are difficult to calculate accurately using the cluster approach, since they involve the calculation of solvation energies of the ligands in bulk water (outside the enzyme), something that could be difficult to reproduce using implicit solvent models. Another complication is the accurate estimation of the entropy effects involved in this process. Nevertheless, we here provide some estimation of the energy involved in this ligand exchange process.

Using an unconstrained small model of the tungsten center, consisting of only truncated models of the pterin ligands (see Supporting Information, Fig. SI2), we found that dissociating the water molecule from the tungsten is slightly exothermic (ca 2 kcal/mol), which means that the replacement of the water by formaldehyde is very feasible.

However, in the large model (*A-React*) the situation is quite different, since the water ligand always loses a proton to Glu308. Because of this, the ligand exchange process (effectively going from *A-React* to *D-React*) is found to be endothermic by up to 16 kcal/mol.

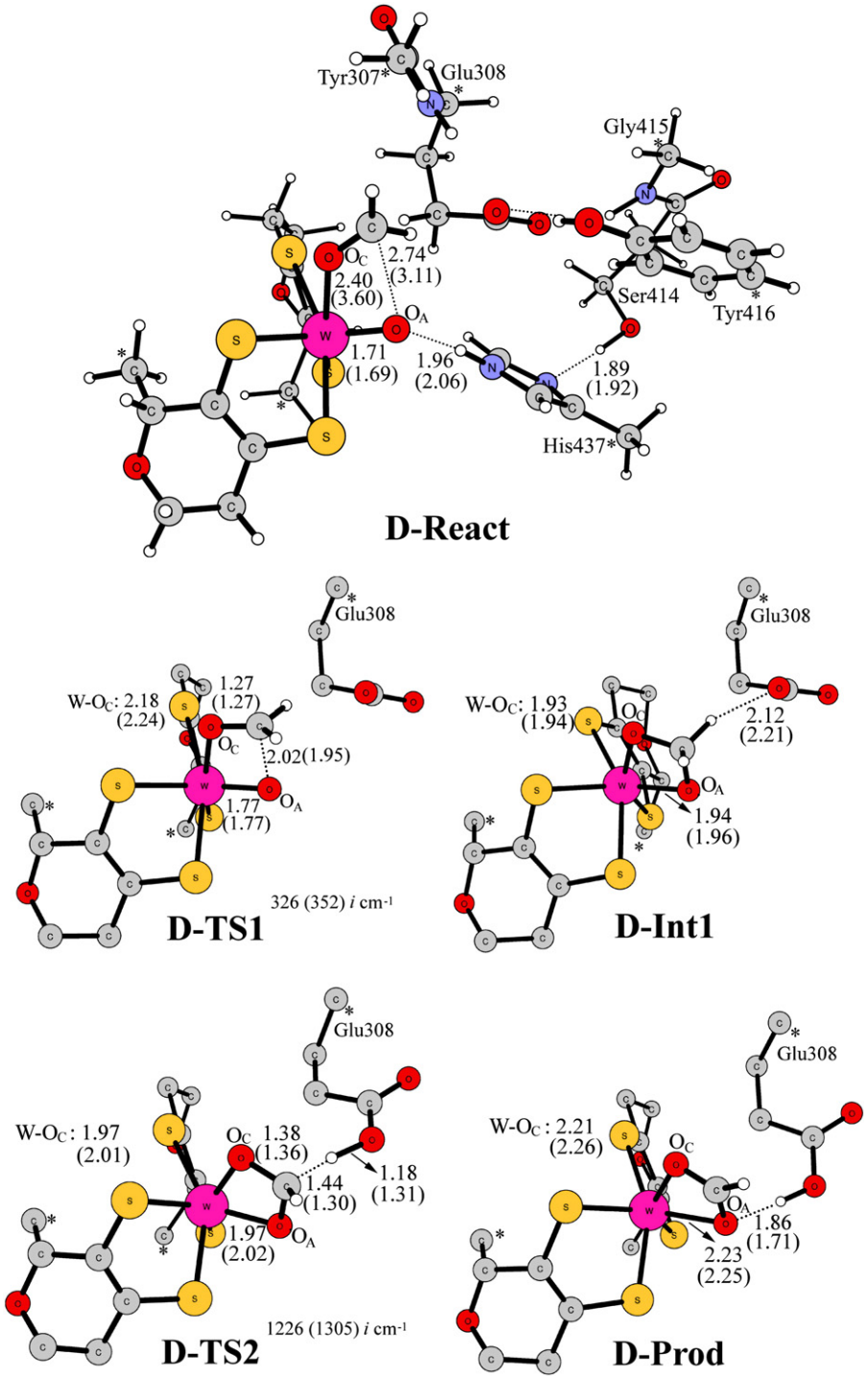


**Fig. 8.** Optimized geometries of stationary points along reaction pathway *D*. For clarity, the full model is shown only for *D-React*. For the other stationary points, some residues and hydrogen atoms are omitted.

Another way to estimate the exchange energy is by using the following equation:

$$A\text{-}React\ (\varepsilon = 4) \rightarrow D\text{-}React\ (\varepsilon = 4) + H_2O\ (\text{in water})$$

The solvation energy of a water molecule in bulk water has been estimated to 14 kcal/mol [77,78], which then would give an endothermicity of ca 12 kcal/mol according to this equation. Again, this large endothermicity is due to the proton transfer from the water ligand to Glu308 in *A-React*.

These estimations, although quite crude, suggest that there could be some energetic penalty to replace the water ligand by the formaldehyde substrate. This energy will lead to somewhat higher overall barriers, which could explain why the barriers calculated for pathway *D* are somewhat underestimated compared to the experimental rates.

## 5. Conclusions

We have in the present paper investigated the reaction mechanism of tungsten-dependent formaldehyde ferredoxin oxidoreductase using a quantum chemical cluster model of the active site. Several possible reaction pathways were considered. Pathways *A*, *B*, and *C*

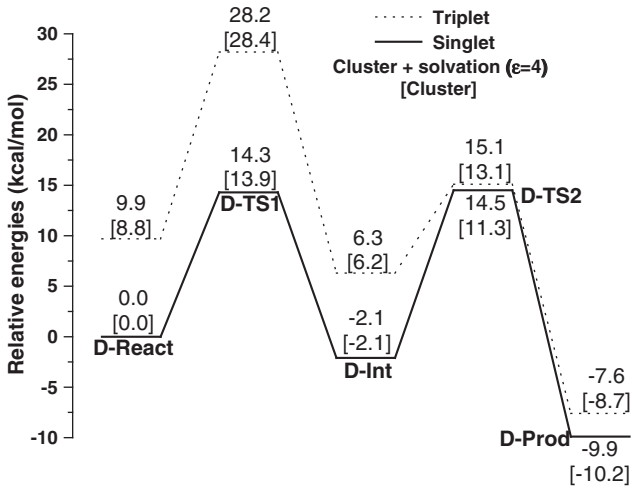


**Fig. 9.** Calculated potential energy profile for pathway *D*.

assume a second-shell mechanism and are shown to be associated with high energy barriers.

In particular, nucleophilic attack on the formaldehyde by a tungsten-bound hydroxide and hydride transfer of the resulting intermediate to the W-oxo group (pathway *A*) have barriers that are higher than 30 kcal/mol. Nucleophilic attack by $W^{VI}$=O, on the other hand, has a feasible barrier (pathway *B*), but the following hydride transfer has again a very high barrier. Also the alternative proton transfer to Glu308 coupled with a two-electron reduction of the metal (pathway *C*) is shown to have a high energy barrier.

Instead, in the preferred mechanism (pathway *D*), it is shown that the aldehyde substrate binds in the first ligand shell of the tungsten. The $W^{VI}$=O then performs the nucleophilic attack on the formaldehyde carbon to form a tetrahedral intermediate. Glu308 functions as a general base to take a proton from the tetrahedral intermediate, in concomitant with two-electron reduction of $W^{VI}$ affording $W^{IV}$. This pathway has feasible energetic barriers that are in reasonable agreement with experimental rate constants. More calculations are currently underway to explain the different behavior observed for molybdenum compared to tungsten for this enzyme.

*Abbreviations*

| | |
|---|---|
| AH | acetylene hydratase |
| AOR | aldehyde oxidoreductase |
| CPCM | conductor-like polarizable continuum model |
| FDH | formate dehydrogenase |
| FOR | formaldehyde ferredoxin oxidoreductase |
| GAPOR | glyceraldehyde-3-phosphate ferredoxin oxidoreductase |
| QM/MM | quantum mechanics and molecular mechanics |
| WOR4 | tungsten-containing oxidoreductase number four |
| WOR5 | tungsten-containing oxidoreductase number five |
| ZPE | Zero-point energy |

## Acknowledgements

F.H. gratefully acknowledges financial support from The Swedish Research Council (Grants 621-2009-4736 and 622-2009-371) and computer time from the PDC Center for High Performance Computing. This work was also supported by grants from the National Natural Science Foundation of China (Grant 20873008).

## Appendix A. Supplementary data

Supplementary data to this article can be found online at doi:10.1016/j.jinorgbio.2011.03.020.

## References

[1] M.K. Johnson, D.C. Rees, M.W.W. Adams, Chem. Rev. 96 (1996) 2817–2839.
[2] J. McMaster, J.H. Enemark, Curr. Opin. Chem. Biol. 2 (1998) 201–207.
[3] N.P. L'vov, A.N. Nosikov, A.N. Antipov, Biochemistry (Moscow) 67 (2002) 234–239.
[4] J.H. Enemark, J.J.A. Cooney, Chem. Rev. 104 (2004) 1175–1200.
[5] C.D. Brondino, M.J. Romão, I. Moura, J.J. Moura, Curr. Opin. Chem. Biol. 10 (2006) 109–114.
[6] H. Sugimoto, H. Tsukube, Chem. Soc. Rev. 37 (2008) 2609–2619.
[7] L.E. Bevers, P.-L. Hagedoorn, W.R. Hagen, Coord. Chem. Rev. 253 (2009) 269–290.
[8] M.J. Romão, Dalton Trans. (2009) 4053–4068.
[9] S. Mukund, M.W.W. Adams, J. Biol. Chem. 266 (1991) 14208–14216.
[10] A. Kletzin, S. Mukund, T.L. Kelly-Crouse, M.K. Chan, D.C. Rees, M.W.W. Adams, J. Bacteriol. 177 (1995) 4817–4819.
[11] R. Roy, S. Mukund, G.J. Schut, D.M. Dunn, R. Weiss, M.W.W. Adams, J. Bacteriol. 181 (1999) 1171–1180.
[12] S. Mukund, M.W.W. Adams, J. Biol. Chem. 270 (1995) 8389–8392.
[13] J. van der Oost, G. Schut, S.W.M. Kengen, W.R. Hagen, M. Thomm, W.M. de Vos, J. Biol. Chem. 273 (1998) 28149–28154.
[14] R. Roy, M.W.W. Adams, J. Bacteriol. 184 (2002) 6952–6956.
[15] L.E. Bevers, E. Bol, P.-L. Hagedoorn, W.R. Hagen, J. Bacteriol. 187 (2005) 7056–7061.
[16] G. Fiala, K.O. Stetter, Arch. Microbiol. 145 (1986) 56–61.
[17] M.K. Chan, S. Mukund, A. Kletzin, M.W.W. Adams, D.C. Rees, Science 267 (1995) 1463–1469.
[18] Y. Hu, S. Faham, R. Roy, M.W.W. Adams, D.C. Rees, J. Mol. Biol. 286 (1999) 899–914.
[19] A.F. Arendsen, M. de Vocht, Y.B.M. Bulsink, W.R. Hagen, J. Biol. Inorg. Chem. 1 (1996) 292–296.
[20] B.P. Koehler, S. Mukund, R.C. Conover, I.K. Dhawan, R. Roy, M.W.W. Adams, M.K. Johnson, J. Am. Chem. Soc. 118 (1996) 12391–12405.
[21] I.K. Dhawan, R. Roy, B.P. Koehler, S. Mukund, M.W.W. Adams, M.K. Johnson, J. Biol. Inorg. Chem. 5 (2000) 313–327.
[22] P.L. Hagedoorn, T. Chen, I. Schröder, S.R. Piersma, S. de Vries, W.R. Hagen, J. Biol. Inorg. Chem. 10 (2005) 259–269.
[23] E. Bol, L.E. Bevers, P.-L. Hagedoorn, W.R. Hagen, J. Biol. Inorg. Chem. 11 (2006) 999–1006.
[24] E. Bol, N.J. Broers, W.R. Hagen, J. Biol. Inorg. Chem. 13 (2008) 75–84.
[25] L.J. Steward, S. Bailer, B. Bennett, J.M. Charnock, C.D. Garner, A.S. McAlpine, J. Mol. Biol. 299 (2000) 593–600.
[26] J. Buc, C.-L. Santini, R. Giordani, M. Czjzek, L.-F. Wu, G. Giordano, Mol. Microbiol. 32 (1999) 159–168.
[27] P.A. Bertram, R.A. Schmitz, D. Linder, R.K. Thauer, Arch. Microbial. 161 (1994) 220–228.
[28] J.A. Vorholt, M. Vaupel, R.K. Thauer, Mol. Microbiol. 23 (1997) 1033–1042.
[29] M. Boll, B. Schink, A. Messerschmidt, P.M.H. Kroneck, Biol. Chem. 386 (2005) 999–1006.
[30] M.J. Romão, M. Archer, I. Moura, J.J.G. Moura, J. LeGall, R. Engh, M. Schneider, P. Hof, R. Huber, Science 270 (1995) 1170–1176.
[31] R. Huber, P. Hof, R.O. Duarte, J.J.G. Moura, I. Moura, M.-Y. Liu, J. LeGall, R. Hille, M. Archer, M.J. Romão, Proc. Natl. Acad. Sci. U. S. A. 93 (1996) 8846–8851.
[32] M.J. Romão, N. Rösch, R. Huber, J. Biol. Inorg. Chem. 2 (1997) 782–785.
[33] J.M. Rebelo, J.M. Dias, R. Huber, J.J.G. Moura, M.J. Romão, J. Biol. Inorg. Chem. 6 (2001) 791–800.
[34] S. Metz, D. Wang, W. Thiel, J. Am. Chem. Soc. 131 (2009) 4628–4640.
[35] M.R. Bray, R.J. Deeth, J. Chem. Soc., Dalton Trans. (1997) 1267–1268.
[36] P. Ilich, R. Hille, Inorg. Chim. Acta 263 (1997) 87–93.
[37] A.A. Voityuk, K. Albert, M.J. Romão, R. Huber, N. Rösch, Inorg. Chem. 37 (1998) 176–180.
[38] P. Ilich, R. Hille, J. Phys. Chem. B 103 (1999) 5406–5412.
[39] P. Ilich, R. Hille, J. Am. Chem. Soc. 124 (2002) 6796–6797.
[40] X.H. Zhang, Y.D. Wu, Inorg. Chem. 44 (2005) 1466–1471.
[41] T. Amano, N. Ochi, H. Sato, S. Sakaki, J. Am. Chem. Soc. 129 (2007) 8131–8138.
[42] S. Metz, W. Thiel, J. Am. Chem. Soc. 131 (2009) 14855–14902.
[43] S. Metz, W. Thiel, J. Phys. Chem. B 114 (2010) 1506–1517.
[44] J.M. Dieterich, H.-J. Werner, R.A. Mata, S. Metz, W. Thiel, J. Chem. Phys. 132 (2010) 035101.
[45] C.E. Webster, M.B. Hall, J. Am. Chem. Soc. 123 (2001) 5820–5821.
[46] M. Kaupp, Angew. Chem. Int. Ed. 43 (2004) 546–549.
[47] J.P. McNamara, J.A. Joule, I.H. Hillier, C.D. Garner, Chem. Commun. (2005) 177–179.
[48] M. Leopoldini, N. Russo, M. Toscano, M. Dulak, T.A. Wesolowski, Chem. Eur. J. 12 (2006) 2532–2541.
[49] K. Pal, P.K. Chaudhury, S. Sarkar, Chem. Asian J. 2 (2007) 956–964.
[50] M. Leopoldini, S.G. Chiodo, M. Toscano, N. Russo, Chem. Eur. J. 14 (2008) 8647–8681.
[51] M. Hofmann, Inorg. Chem. 47 (2008) 5546–5548.
[52] M. Hofmann, J. Biol. Inorg. Chem. 14 (2009) 1023–1035.
[53] N. Cerqueira, P.J. Gonzalez, C.D. Brondino, M.J. Romão, C.C. Romão, I. Moura, J.J. Moura, J. Comput. Chem. (2009) 2466–2484.
[54] A.D. Becke, J. Chem. Phys. 98 (1993) 5648–5652.
[55] C. Lee, W. Yang, R.G. Parr, Phys. Rev. B 37 (1988) 785–789.
[56] M.R.A. Blomberg, P.E.M. Siegbahn, J. Phys. Chem. B 105 (2001) 9375–9386.
[57] F. Himo, P.E.M. Siegbahn, Chem. Rev. 103 (2003) 2421–2456.
[58] L. Noodleman, T. Lovell, W.-G. Han, J. Li, F. Himo, Chem. Rev. 104 (2004) 459–508.

[59] P.E.M. Siegbahn, T. Borowski, Acc. Chem. Res. 39 (2006) 729–738.
[60] F. Himo, Theo. Chem. Acc. 116 (2006) 232–240.
[61] M.J. Ramos, P.A. Fernandes, Acc. Chem. Res. 41 (2008) 689–698.
[62] F. Himo, P.E.M. Siegbahn, J. Biol. Inorg. Chem. 14 (2009) 643–651.
[63] M.R.A. Blomberg, P.E.M. Siegbahn, Biochim. Biophys. Acta 1797 (2010) 129–142.
[64] R.-Z. Liao, J.-G. Yu, F. Himo, Proc. Natl. Acad. Sci. U. S. A. 107 (2010) 22523–22527.
[65] Gaussian 03 (Revision D.01), M.J. Frisch, G.W. Trucks, H.B. Schlegel, G.E. Scuseria, M.A. Robb, J.R. Cheeseman, J.A. Montgomery Jr., T. Vreven, K.N. Kudin, J.C. Burant, J.M. Millam, S.S. Iyengar, J. Tomasi, V. Barone, B. Mennucci, M. Cossi, G. Scalmani, N. Rega, G.A. Petersson, H. Nakatsuji, M. Hada, M. Ehara, K. Toyota, R. Fukuda, J. Hasegawa, M. Ishida, T. Nakajima, Y. Honda, O. Kitao, H. Nakai, M. Klene, X. Li, J.E. Knox, H.P. Hratchian, J.B. Cross, C. Adamo, J. Jaramillo, R. Gomperts, R.E. Stratmann, O. Yazyev, A.J. Austin, R. Cammi, C. Pomelli, J.W. Ochterski, P.Y. Ayala, K. Morokuma, G.A. Voth, P. Salvador, J.J. Dannenberg, V.G. Zakrzewski, S. Dapprich, A.D. Daniels, M.C. Strain, O. Farkas, D.K. Malick, A.D. Rabuck, K. Raghavachari, J.B. Foresman, J.V. Ortiz, Q. Cui, A.G. Baboul, S. Clifford, J. Cioslowski, B.B. Stefanov, G. Liu, A. Liashenko, P. Piskorz, I. Komaromi, R.L. Martin, D.J. Fox, T. Keith, M.A. Al-Laham, C.Y. Peng, A. Nanayakkara, M. Challacombe, P.M.W. Gill, B. Johnson, W. Chen, M.W. Wong, C. Gonzalez, J.A. Pople, Gaussian, Inc., Pittsburgh, PA, 2004.
[66] L.E. Roy, P.J. Hay, R.L. Martin, J. Chem. Theory Comput. 4 (2008) 1029–1031.
[67] K.G. Dyall, J. Phys. Chem. A 104 (2000) 4077–4083.
[68] M.F.A. Hendrickx, V.S. Mironov, L.F. Chibotaru, A. Ceulemans, Inorg. Chem. 43 (2004) 3142–3150.
[69] A. Klamt, G. Schüürmann, J. Chem. Soc., Perkin. Trans. 2 (1993) 799–805.
[70] J. Andzelm, C. Kölmel, A. Klamt, J. Chem. Phys. 103 (1995) 9312–9320.
[71] V. Barone, M. Cossi, J. Phys. Chem. A 102 (1998) 1995–2001.
[72] M. Cossi, N. Gega, G. Scalmani, V. Barone, J. Comput. Chem. 24 (2003) 669–691.
[73] R. Sevastik, Himo, F. Bioorg. Chem. 35 (2007) 444–457.
[74] K.H. Hopmann, F. Himo, J. Chem. Theor. Comp. 4 (2008) 1129–1137.
[75] P. Georgieva, F. Himo, J. Comput. Chem. 31 (2010) 1707–1714.
[76] Y. Zhao, B.J. Lynch, D.G. Truhlar, J. Phys. Chem. A 108 (2004) 2715–2719.
[77] P.E.M. Siegbahn, Philos. Trans. R. Soc. London, Ser. B 363 (2008) 1221–1228.
[78] P.E.M. Siegbahn, M.R.A. Blomberg, J. Phys. Chem. A 112 (2008) 12772–12780.